AIP Advances

Ferroelectric polymer-ceramic composite thick films for energy storage applications

Paritosh Singh, Hitesh Borkar, B. P. Singh, V. N. Singh, and Ashok Kumar

Citation: AIP Advances **4**, 087117 (2014); doi: 10.1063/1.4892961
View online: http://dx.doi.org/10.1063/1.4892961
View Table of Contents: http://scitation.aip.org/content/aip/journal/adva/4/8?ver=pdfcov
Published by the AIP Publishing

AIP ADVANCES **4**, 087117 (2014)

Ferroelectric polymer-ceramic composite thick films for energy storage applications

Paritosh Singh, Hitesh Borkar, B. P. Singh, V. N. Singh, and Ashok Kumar[a]
CSIR-National Physical Laboratory, Dr. K. S. Krishnan Marg, New Delhi 110012, India

(Received 11 June 2014; accepted 31 July 2014; published online 11 August 2014)

We have successfully fabricated large area free standing polyvinylidene fluoride -Pb($Zr_{0.52}Ti_{0.48}$)O_3 (PVDF-PZT) ferroelectric polymer-ceramic composite (wt% 80–20, respectively) thick films with an average diameter (d) ~0.1 meter and thickness (t) ~50 μm. Inclusion of PZT in PVDF matrix significantly enhanced dielectric constant (from 10 to 25 at 5 kHz) and energy storage capacity (from 11 to 14 J/cm^3, using polarization loops), respectively, and almost similar leakage current and mechanical strength. Microstructural analysis revealed the presence of α and β crystalline phases and homogeneous distribution of PZT crystals in PVDF matrix. It was also found that apart from the microcrystals, well defined naturally developed PZT nanocrystals were embedded in PVDF matrix. The observed energy density indicates immense potential in PVDF-PZT composites for possible applications as green energy and power density electronic elements. [http://dx.doi.org/10.1063/1.4892961]

I. INTRODUCTION

There have been needs of inherent self-powered energy storage devices which can replace batteries to power the microelectronic devices like wireless sensors, mobile communication systems, electric vehicles, health monitoring systems and pulse power applications. Systems which can harness energy from natural sources have been of great interest among the researchers from past few decades. Two criteria are very important for any energy storage devices, the first one is how much energy can it store per unit of its volume or mass (energy density) and secondly the power density available to load. The power density refers how quick a system can discharge its stored energy to the external load. Our concern is to develop a system which shows higher energy storage ability and simultaneously high discharge capacity (power density). Although a system having superior energy density and power density is not possible at the same time so there is a compromise. In particular, conventional batteries have very high energy density, but very slow discharge capacity, on the other hand the dielectric capacitors have high discharge capacity, but very low energy density.[1]

The conversion from mechanical and vibrational energy from natural sources like wind, waves or human motions into electrical energy have been of a great interest in scientific community.[2–6] One way to harness electrical energy from sources of mechanical vibrations is to utilize the piezoelectric properties of ferroelectric materials. This work investigates the ferroelectric polymer-ceramic composite for its property to store high energy. The monomer unit of this polymer is CH_2-CF_2 is semi crystalline in nature, half crystalline and half amorphous. The crystalline region consists of at least four crystal polymorphs named α, β, γ and δ.[7,8] Among four polymorphs, α phase is most stable nonpolar phase having conformation structure TGTG (T-trans, G-gauche).[9] The β phase of the PVDF polymer has planer all trans (TTTT) conformation (Fig. 1).[9] In β phase, the H and F atoms are attached in the chain in such a way the dipole moments associated with two C-H and two C-F bonds add up and align in the direction perpendicular to the carbon backbone to give higher dipole

[a]Corresponding Author: Dr. Ashok Kumar (ashok553@nplindia.org).

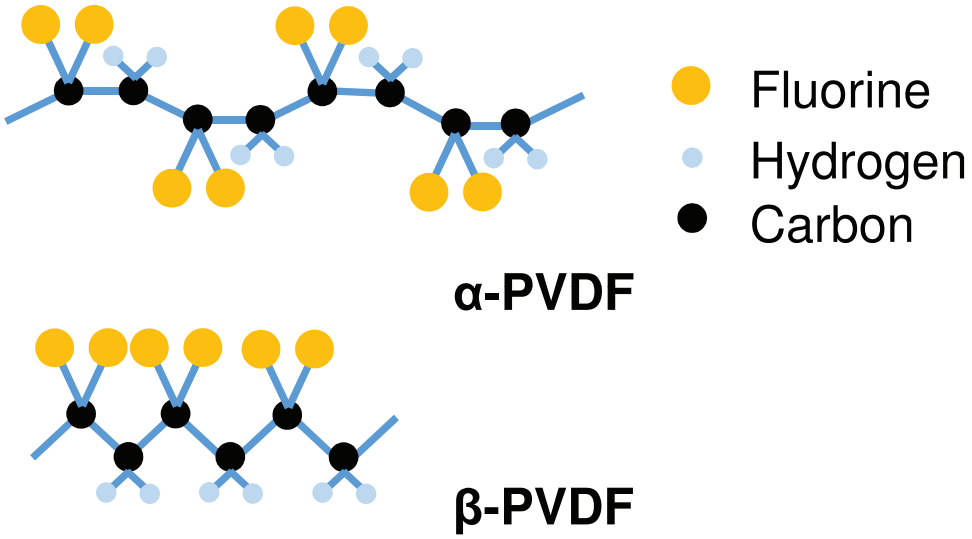

FIG. 1. Molecular structure of α and β PVDF.

moments per unit cell.[10] It is the β phase which attracts the researchers for its high piezoelectric and ferroelectric properties. So lots of research is going on for yielding high β-phase content in the material. Different phases exist in PVDF depending on various processing parameters like type of solvent in solution casting, solvent evaporation temperatures, fillers in the polymer matrix, stretching load and annealing to make stable β-phase, controlled annealing or electrical poling of the prepared PVDF film.[11–13]

The need of high energy density storage system has led to the development of ferroelectric polymer-ceramic composite system. Polymer-ceramic system combines the property of both ferroelectric polymer and ceramic fillers. PVDF polymer has light weight, larger chain flexibility, good mechanical properties, chemical and electrical resistance, availability and good process ability. Due to good chain flexibility, PVDF based energy harvester systems can sustain larger vibration. Inclusion of high dielectric constant ceramic fillers in the polymer matrix exhibits enhanced dielectric behavior and piezoelectric response of the polymer-ceramic composite material in comparison to ferroelectric polymer.[14,15] Polymer-ceramic composite system combines high dielectric constant (ε) and stiffness of ceramics and flexibility, elasticity and high dielectric breakdown of ferroelectric polymers.

The existing technology of polymer capacitor has potential to store an energy density <3 J/cm^3,[16] however the future pulsed power electronic industries required a capacitor with minimum energy density equivalent to the existing electrochemical capacitor $\sim$18–29 J/cm^3 and very fast discharge capacity.[17] Significant progress has been made to achieve the above mentioned target; however, reliable data for large area scalable at industrial level are missing. Tomer *et al.* have shown $\sim$19 J/cm^3 energy density for PVDF-HFP comonomers and kaolinite-clay composites.[18] Penghao Hu *et al.* illustrate low energy density ($\sim$3–4 J/cm^3) for (Ba,Sr)TiO_3/poly(vinylidene-fluoride-trifluoroethylene), flexible nanocomposites.[19] Literature survey indicates that numerous investigations on ceramic-polymer composites on PVDF and PVDF-co-polymer matrix has been carried out, such as $BaTiO_3$,[20] $Pb(Mg_{1/3}Nb_{2/3})O_3$–$PbTiO_3$,[21] $Pb(Zr_xTi_{1-x})O_3$ (PZT),[22] and etc., however, reproducibility, large scale production, energy storage capability, and fast energy release properties, still need further rigorous systematic study.

In this study we have used micron size lead-zirconate-titante particles $Pb(Zr_{0.52}Ti_{0.48})O_3$ (PZT) ($\varepsilon \sim 400$, density $\sim$ 7.5 g/cm^3) as filler in PVDF matrix ($\varepsilon \sim$ 8–10, density $\sim$ 1.78 g/cm^3). The problem in getting higher dielectric constant with inclusion of PZT filler into polymer matrix also increases dielectric loss and weak mechanical properties in composite system as we increase the content of PZT in polymer. In order to compromise between dielectric constant and tangent loss,

PVDF-PZT composite of wt%80–20, respectively, was fabricated and investigated for various functional properties.

II. METHODS

PVDF powder was procured from Alfa Aesar India Pvt. Ltd and PZT powder was synthesized in the laboratory by conventional solid state reaction technique. The PVDF and PVDF-PZT composite thick films have been prepared by solution cast method. For PVDF thick film, PVDF powder was dissolved in N, N-Dimethylformamide (DMF) solvent by magnetic stirring for 6 hours at 50 °C. The dissolved solution then poured into uncovered petri dish and this assembly was kept inside microwave oven at 100°C for 12 hours for crystallization. In this time duration the solvent completely evaporated and a free standing PVDF film of thickness 50 μm obtained. For PVDF-PZT nano-composite film, we have taken PVDF powder and PZT nanoparticles in the ratio of wt% 80–20 respectively. The mixture was dispersed in DMF solvent by ultra-sonication for 50 minutes at 40 °C. The PVDF-PZT solution then magnetically stirred for 6 hours at 50 °C. Now the obtained solution was sonicated again for 50 minutes and the rest process is same as of the casting of PVDF film. We obtained PVDF-PZT free standing film of thickness 50μm. X-Ray diffraction measurement of PVDF and PVDF-PZT composite thick films were carried out by using CuK_α radiation ($\lambda = 1.5460$ Å) over a wide range of θ–2θ Bragg angles. Raman spectra were recorded on Renishaw in Via Reflex Raman spectrometer, UK, with an excitation source of 785 nm. Scanning electron microscopy (SEM) technique was used to understand the matrix using Zeiss EVO MA-10, Scanning Electron Microscope. To check mechanical properties, tensile testing has been carried out in INSTRON tensile testing machine with strain rate of 0.5 mm/minute. Temperature dependent dielectric constant and tangent loss were carried out by using LCR meter (4200-SCS Analyzer) at oscillating amplitude of 0.5 V over wide range of frequencies (1 kHz-1 MHz). Polarization-electric field (P-E) hysteresis loops were measured on Radiant Ferroelectric Tester for different voltage cycles at 10 Hz.

III. RESULTS AND DISCUSSION

A. X-Ray Diffraction Analysis

X-ray diffraction (XRD) studies have been carried out on both PVDF and PVDF-PZT composite free standing thick films casted at temperature 100°C, as shown in the Fig. 2(a) and 2(b). It is evident from Figure 2(a) that the peaks at 2θ corresponding to 18.5°, and 26.5° present in XRD pattern indicates the presence of α-phase.[23] Presence of high intense peak at 20.2° confirms the presence of β-phase in PVDF film.[24] Other XRD peaks at 36.1°, 43.2° and 57.4° are indexed to the corresponding β-phase of PVDF film and α-phase corresponds to 39.5° and 48.6°.Thus the neat PVDF film developed by solvent casting using solvent N,N-Dimethyl formamide at temperature 100°C shows the presence of both α and β phase which agree with the published literature by researchers.[25,26] XRD pattern thus indicates the semi-crystalline nature of PVDF polymer film. The XRD spectra of PVDF-PZT composite system with PZT chemical compositions $Pb(Zr_{0.52}Ti_{0.48})O_3$ have been shown in Fig. 2(b), indexing and peak positions matched with the JCPDS file # 33–0784. The obtained XRD peaks of PZT in the composite matched with the PZT peaks reported near the morphotropic phase boundary (MPB) and suggests the tetragonal crystal structure with the lattice parameters, a = b = 0.4036 nm, c = 0.4146 nm, corresponding phase matched well with the reported data (JCPDS: 33–0784). It is observed that there is no shift in PZT peaks position due to the presence of PVDF matrix.[27,28] It can be clearly seen in the XRD spectra of the composite film that most XRD peaks of PVDF is dominated by PZT peaks. For further confirmation of α and β phases present in the PVDF and composite, Raman analysis have been carried out.

B. Raman Analysis

Figures 3(a)–3(d) represents the Raman spectra of PVDF and PVDF-PZT nano-composite thick films from 100 cm^{-1} -1100 cm^{-1}. Three major Raman modes at 798, 812 and 839 cm^{-1} of PVDF

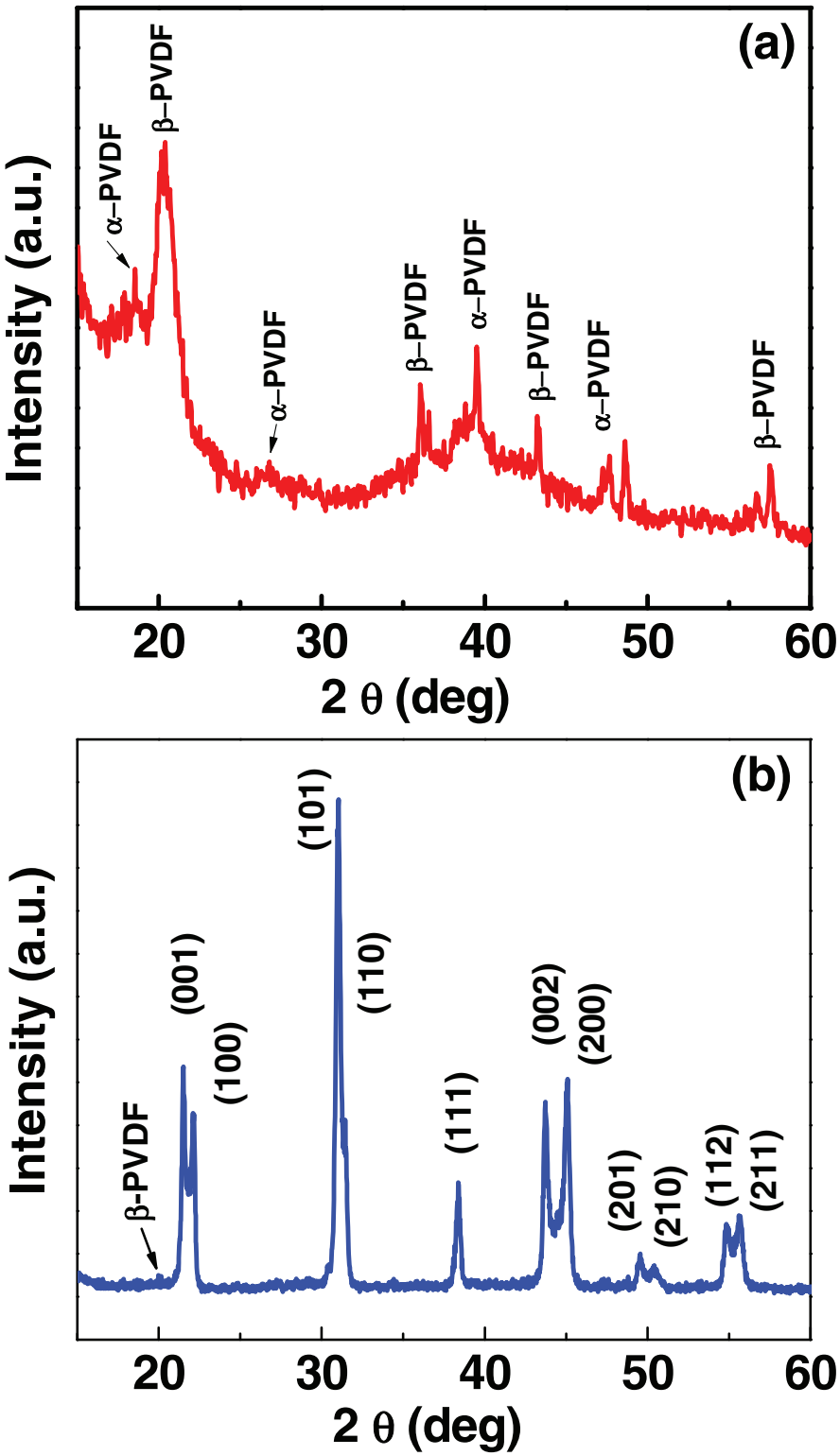

FIG. 2. X-ray diffraction pattern of (a) pure PVDF film and (b) PVDF-PZT composite film casted at 100°C. The XRD pattern of pure PVDF shows the existence of α and β PVDF phases.

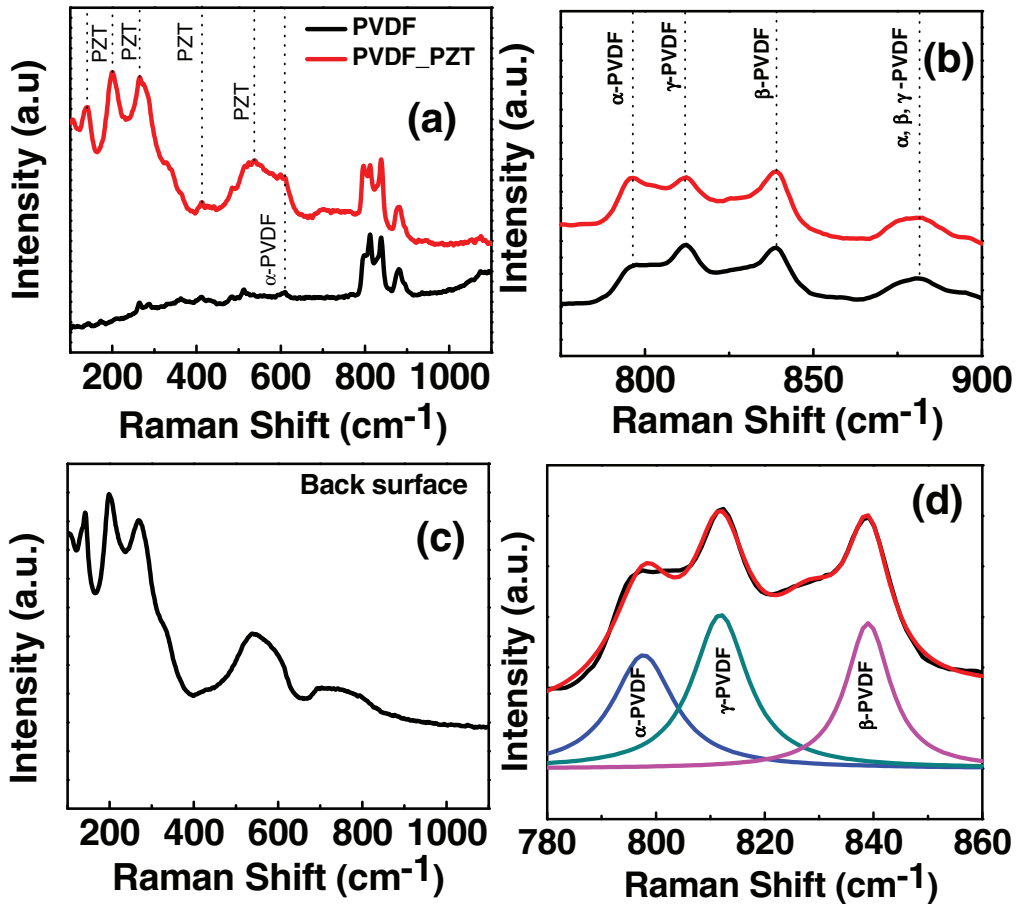

FIG. 3. Raman Spectra of PVDF and PVDF-PZT composite films. (a) Raman spectra in frequency range 100 cm^{-1} to 1100 cm^{-1} for both films, (b) Raman spectra in frequency range 780 cm^{-1} to 900 cm^{-1}, revealing the α, β and γ phases of PVDF, (c) Raman spectra of back surface of PVDF-PZT composite system, mainly showing PZT bands in frequency range 100 cm^{-1} to 1100 cm^{-1} and (d) three major Raman modes at 798, 812 and 839 cm^{-1} of PVDF film have been analyzed by damped harmonic oscillator model (DHO).

and PVDF-PZT films have been analyzed by damped harmonic oscillator model (DHO).[29] These phonon modes were fitted with the spectral response function.

$$S(\nu) = \sum_i \frac{\chi_{0i}\Gamma_i \nu_{0i}^2 \nu}{(\nu^2 - \nu_{0i}^2) + \Gamma_i^2 \nu^2} F(\nu, T) \quad (1)$$

where $F(\nu,T) = [n(\nu) + 1]$ (Stokes scattering) and $n(\nu) = [exp(h\nu/\kappa T) - 1]^{-1}$. The parameters in Eq. (1) amplitude χ_0 (in arbitrary units), the mode frequency ν_0, the damping constant Γ, and the temperature T, describe each phonon modes as a damped harmonic oscillator. Intense PVDF Raman bands in the range of 775–860 cm^{-1} are analyzed with DHO model as shown in the Fig. 3(d). The low intensity peak at 798 cm^{-1} represents the presence of α phase of PVDF.[30] Peak at 839 cm^{-1} represents β-phase, in addition of PZT filler in PVDF matrix enhanced the β-phase as can be seen in Fig. 3(b) where the intensity of β-phase mode is relatively higher compare to α-phase.[31,32] Significant amount of γ phase also coexist in both the systems. The Raman band at 812 cm^{-1} corresponds to γ phase of PVDF film matched with the reported results.[30,33] Peaks at 484 and 512 cm^{-1} can be attributed to α and β phases respectively.[34]The Raman peaks at 610 cm^{-1} and 411 cm^{-1} correspond to α phase and 284 cm^{-1} correspond to β phase of PVDF.[35] The broad Raman peak at 881 cm^{-1} represents the presence of all three phases (α, β and γ).[36] The diffused Raman bands appearing from 1074 to 1095 cm^{-1} may be assigned to combination of both α and

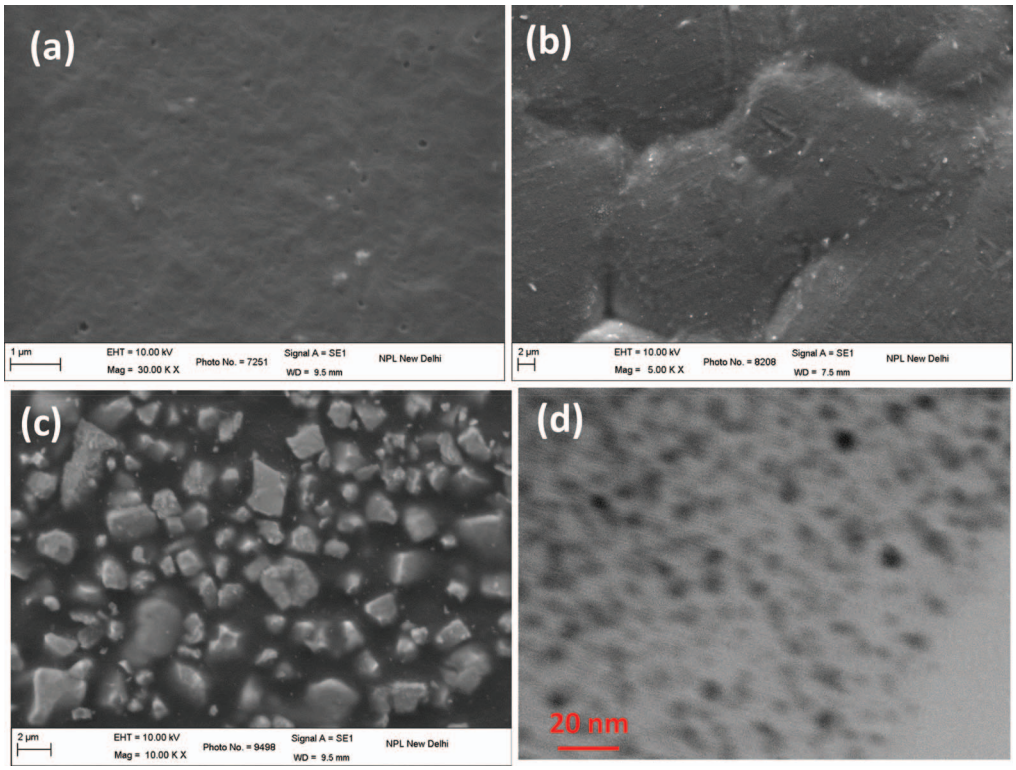

FIG. 4. SEM micrograph of (a) pure PVDF film, (b) PVDF-PZT composite film, (c) back surface of PVDF-PZT composite film, and (d) HRTEM micrograph of PVDF-PZT composite film (∼3–8 nm PZT nanocrystals are embedded in the PVDF matrix)

β phases.[37] Fig. 3(c) shows the Raman spectra of the back surface of the PVDF-PZT film which is completely dominated by the tetragonal PZT Raman bands. It also suggests that the most of the PZT crystals were trapped at the lower portion of the PVDF matrix during crystallization as evidenced from the SEM images of the back portion of the composite. These PZT modes are well established and explained for the tetragonal PZT phase. The Raman bands below the 150 cm^{-1} is known as external modes of the materials, particularly for PZT, it is related to the Pb-lattice modes, however, modes above than 150 cm^{-1} represents the internal bands such as bending, torsion, and stretching.[38]

C. Microstructural Analysis

Fig. 4(a)–4(c) shows the SEM images of PVDF and PVDF-PZT composite films, it indicates top surface of both the systems are homogenous without wrinkles, grains, voids, cracks, and deformation. Heavy PZT grains with average size 2–5 μm settled down at the bottom of the PVDF matrix (Fig. 4(d) even after long time ultrasonication. It may be due to high density of PZT particles.[39,40] It is expected to be uniform distribution of the particles on the bottom surface of the polymer film which is supported by SEM/TEM images. Fig. 4(d) shows the high resolution transmission electron micrograph of PVDF-PZT nano-composite. We observed an interesting feature in the PVDF-PZT matrix, apart from the micron size crystals, very fine 3–8 nm PZT crystals evolved during the polymerization and homogeneously distributed to the PVDF networking. The average particle size is around 5–8 nm which can be seen throughout the matrix. Faceting and oscillation of PZT nanoparticles in PVDF matrix have been observed under the constant illumination of electron beam (not shown).

D. Mechanical Characterization

Fig. 5 represents the stress versus strain characteristics of both films. It is found that the Young's modulus of the PVDF film increases with addition of PZT particles and simultaneously

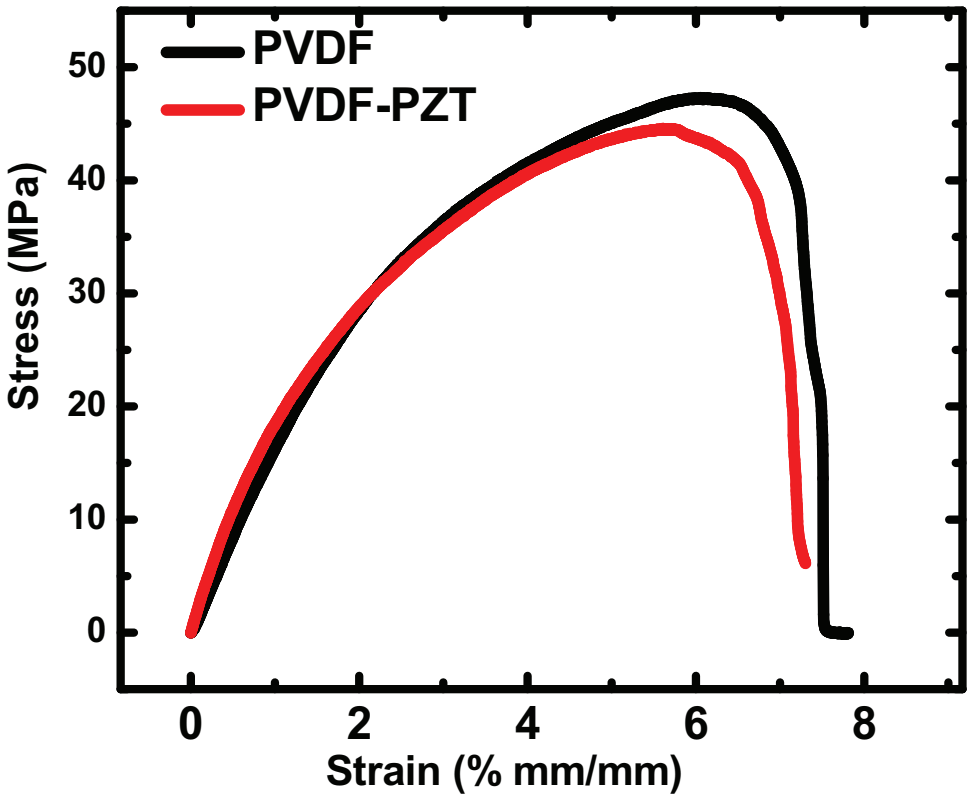

FIG. 5. Stress-strain behavior of PVDF and PVDF-PZT composite system.

tensile strength of the composite film decreases in comparison to neat PVDF film.[41] With 20 wt% PZT in PVDF the Young's modulus and tensile strength was found to be 2.3 GPa and 44.57 MPa respectively whereas it was 1.8 GPa and 47.29 in case of neat PVDF film. Increase in Young's modulus leads to enhanced piezoelectric properties of the composite film.[39] The flexibility of composite film was found to be reduced from 7.8% to 7.3% as it sustains less elongation just before failure.

E. Dielectric Analysis

Fig. 6 represents the dielectric constant and tangent loss (inset) of PVDF and PVDF-PZT composite film over wide range of frequencies. PVDF is a polar polymer which consists of α and β phases which is revealed by XRD analysis and Raman spectra. This polar property of polymer plays a significant role in determining the dielectric properties. In β phase the H and F atoms are aligned in such a manner to give a net dipole moment on the other hand α phase is more stable but nonpolar so this phase does not contribute to polarization.[24] Electronic and atomic polarization are instantaneous which are better able to follow the phase of alternating field in comparison to orientational polarization which takes some time to align the dipoles in the direction of field. So the orientational polarization is the main factor which restricts the dielectric constant at higher frequencies.[42] In general, the dielectric constant of polymer also increases with increase in temperature, in this circumstance, the polymer chain breaks due to thermal agitation. The polar groups will now be freer to align themselves in the direction of changing field. The dielectric loss arises from the inability of dipoles to follow the oscillating electric field. The relaxation (the time to come back of dipoles in their original random orientational state) of dipoles does not occur instantaneously. At higher frequencies the dipoles are not able to keep phase with oscillating field so losses are more at higher frequencies.

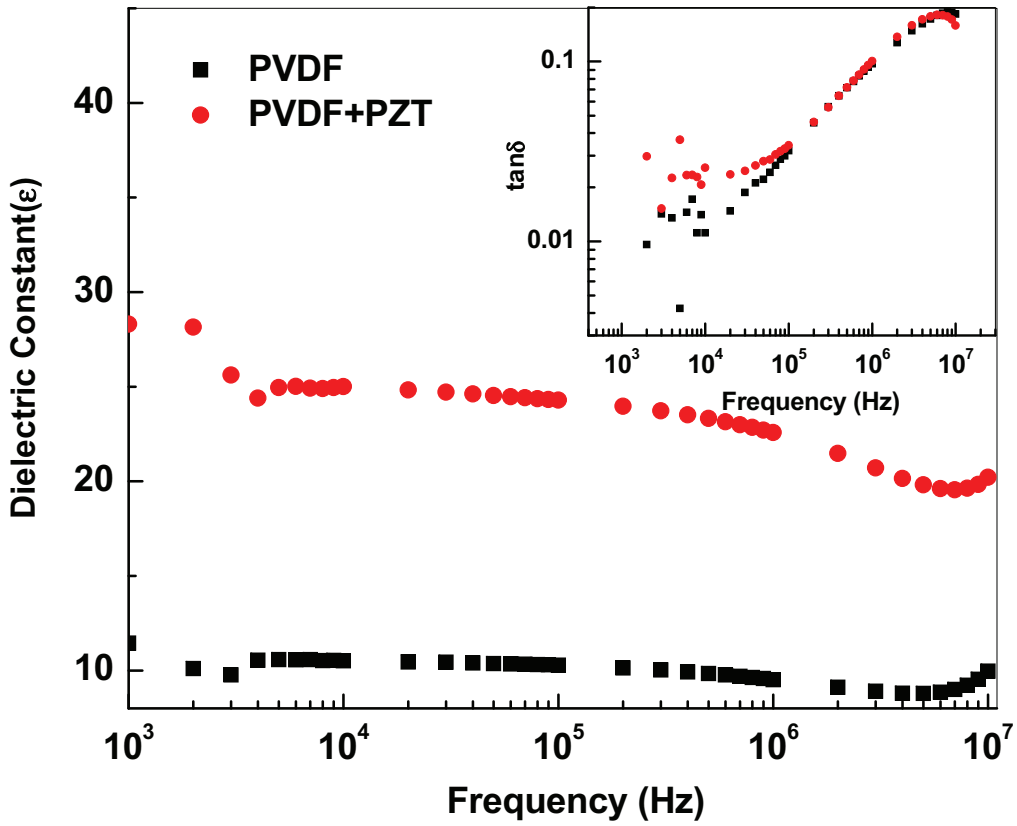

FIG. 6. Frequency dependence dielectric constant and tangent loss (inset) of pure PVDF film and PVDF-PZT composite film at room temperature, from 1 kHz to 10 MHz.

PVDF-PZT composite showed almost 2.5 times increase in dielectric constant with almost similar dielectric loss compared to neat PVDF thick film.[43,44] The increase in dielectric constant of composite is attributed to high dielectric constant of PZT nanoparticles and the interface between particles and polymer matrix. Yamada model predicts the equivalent dielectric constant of two phase polymer-ceramic composite with average ellipsoidal dimension of solid particles.[49] $\varepsilon = \varepsilon_1 \left\{1 + \frac{nq(\varepsilon_2-\varepsilon_1)}{n\varepsilon_1+(\varepsilon_2-\varepsilon_1)(1-q)}\right\}$ where $n = 4\pi/m$, $q = Nv/V$ is the volume fraction of solid particles, ε_1 is the dielectric constant of continuum matrix and ε_2 is the dielectric constant of ellipsoidal solid particles. The experimental value of the dielectric constant of PVDF-PZT (∼25) matched with the theoretical calculation using the Yamada model with n = 10.6. The average spherical/ellipsoidal particles impede the thermal motion of dipoles at higher temperature due to which increase in dielectric constant was observed at elevated temperatures.[45,46] It is noticeable that at higher frequencies loss decreases because the dipoles which are not able to align with field at lower temperature now able to keep in phase with oscillating field.

F. Polarization-Electric Field loops

Hysteresis loop of PVDF and PVDF-PZT nano-composite thick film taken at 10 Hz is presented in Fig. 7. The top and bottom surfaces of both films were silver coated for electrode purpose. The PVDF-PZT nano-composite thick film showed increased saturation polarization in comparison to neat PVDF thick film. In this study the maximum polarization 21.6 μC/cm^2 at electric field 1.8 MV/cm were reported in case of composite whereas this value is around 17 μC/cm^2 at electric field 1.8 MV/cm in neat PVDF film.[47,48]The breakdown field in both cases was comparable, which reached up to 1.8 MV/cm without breakdown (compliance limit ∼1 mA, and the instrument

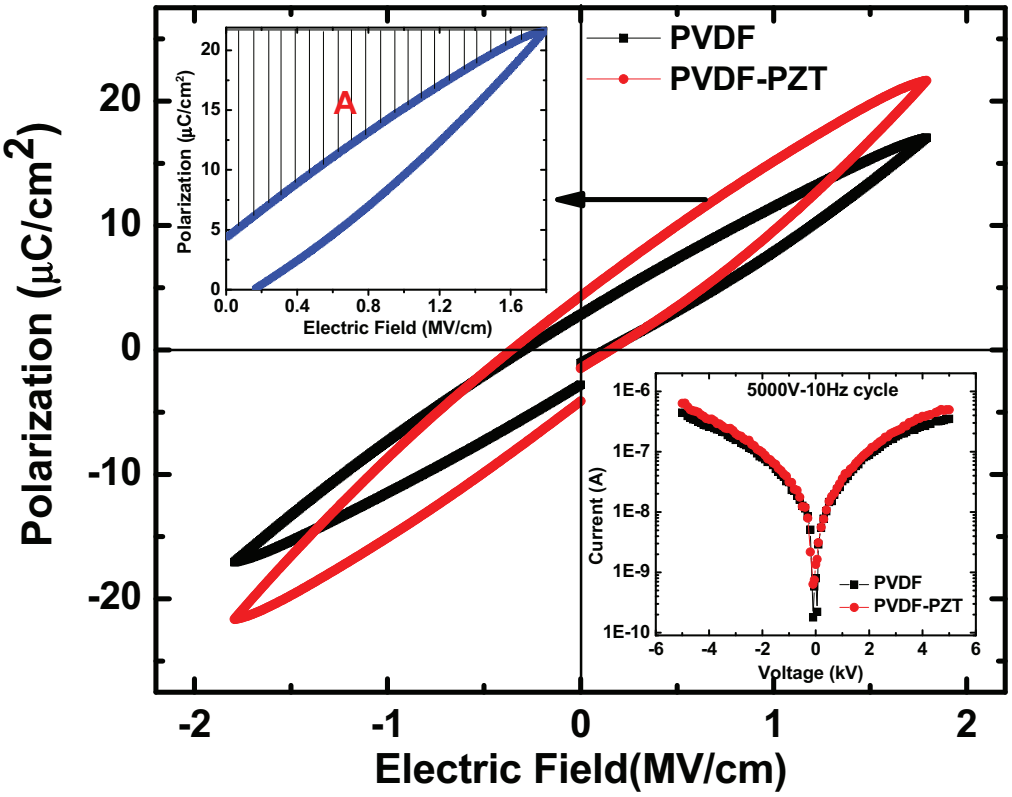

FIG. 7. Electric polarization vs electric field loops (P-E loops) of PVDF and PVDF-PZT composite at an applied field of 1.8 MV/cm at 10 Hz. Current-voltage behavior is shown in inset for 5000 V (∼1 MV/cm) and 10 Hz cycle. Shaded are 'A' is shown in another inset that represents the stored energy density.

limitations). High remnant polarization (P_r) and coercive field develop in PVDF-PZT composite in comparison to PVDF film. In hysteresis plot the current-voltage relationship is also shown in inset which was taken at 5000 V (∼1 MV/cm) and 10 Hz cycle. The range of current suggests the low leakage current for PVDF and PVDF-PZT composite even at high electric field.

G. Energy density properties

Energy storage capacity of PVDF and PVDF-PZT composite films has been represented by the left inset (top) of Fig. 7. This energy density was calculated from the hysteresis loop (polarization-field loop).[49,50] The shaded area (A) in Fig. 7 represents the released energy density (E_R) and the area inside the loop represents the energy loss (E_L). The sum of E_R and E_L represents the total energy density (E_T) stored in the material. The efficiency of the system may be defined as the ratio of released energy density to total stored energy density. In this discussion the general term energy density has been used to refer released/recoverable energy density. To achieve higher energy density in the material, we require three important things. Firstly, the maximum saturation polarization should attain higher value, second, the breakdown field of the film (maximum field that can be sustained by the film) should be high and the last one is remnant polarization should be lower so that the shaded area may become higher. From Fig. 7 the maximum achievable polarization in case of PVDF-PZT composite film with thickness 50 μm is higher in comparison to neat PVDF film. The reason for higher polarization can be attributed to the contribution from the interfaces between PZT nanoparticles filler and polymer matrix. Interfacial regions between PZT filler and PVDF matrix greatly influence the dielectric properties of composites. The dielectric particles get charged due to the Fermi potential equalization of matrix and nanoparticles which causes the buildup

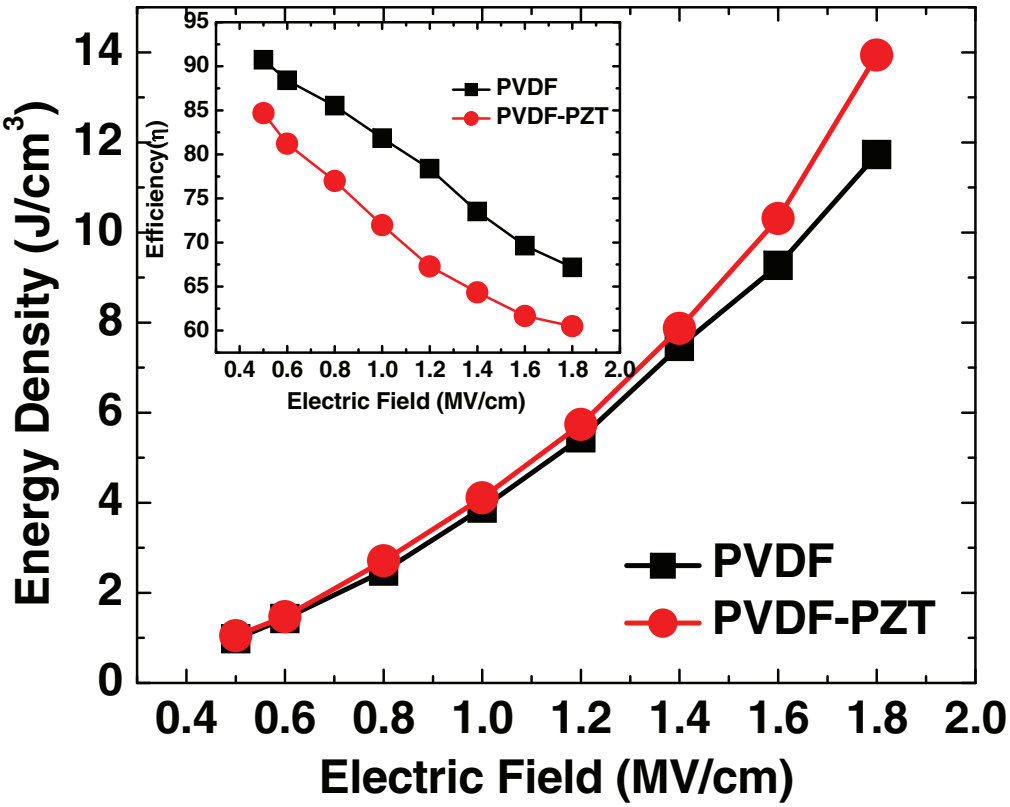

FIG. 8. Energy density of PVDF and PVDF-PZT composite calculated from P-E loops and the corresponding efficiency for both systems (inset).

of charge distribution layer in polymer matrix in the vicinity of charged nanoparticles.[51] Interfacial layers become more conductive than polymer matrix, which prohibits the space charge accumulation and field by rapid discharge through conductive channel. This process improves breakdown field of composite which in turn allows higher degree of polar domains switching and hence enhanced polarization in PVDF-PZT composite.

Fig. 8 shows the variation of stored energy density and efficiency of the system (inset) with applied electric field. It is apparent from the figure 8 that the energy density stored in the 50 μm composite film is increased significantly than the neat PVDF film, however the efficiency of the composite system got slightly decreased due to some extent high energy loss. The composite showed the capacity to store the maximum energy density up to 13.94 J/cm^3.

IV. CONCLUSIONS

The microstructure and the functional properties of PVDF film is influenced with inclusion of PZT micro/nano fillers. Inclusion of polar PZT in PVDF matrix improved the spontaneous polarization, with almost similar breakdown field and leakage current. Young's modulus is enhanced which results in good piezoelectric response although some reduction in tensile strength from 47.29 MPa to 44.57 MPa is also observed. Dielectric constant of composite film is increased (almost 2.5 times) in frequency range 5 kHz-50 kHz in comparison to neat PVDF film with almost similar dielectric loss. Increase in dielectric constant with almost similar breakdown field leads to increase in stored electrical energy density of PVDF-PZT composite to 13.94 J/cm^3.

ACKNOWLEDGMENT

Mr. Paritosh Singh would like to thank Prof. R C Budhani (Director, CSIR-NPL) and Prof. A Dhar for his constant encouragement and CSIR-NPL (AcSIR) for M. Tech fellowship.

Authors would like to thank Prof. Vinay Gupta, Delhi University, and Dr. D. K. Pradhan, NIT Rourkela for their valuable suggestions and experimental supports. Authors would like to thank Mr. K N Sood for SEM imaging and Mr. Dinesh Singh for TEM illustrations.

[1] Thomas Christen and Martin W. Carlen, Journal of Power Sources **91**, 210 (2000).
[2] B. Z. Tian, X. L. Zheng, T. J. Kempa, Y. Fang, N. F. Yu, G. H. Yu, J. L. Huang, and C. M. Lieber, Nature **449**, 885 (2007).
[3] R. S. Yang, Y. Qin, L. M. Dai, and Z. L. Wang, Nat. Nanotechnol. **4**(1), 34 (2009).
[4] J. H. Song, J. Zhou, and Z. L. Wang, Nano Lett. **6**(8), 1656 (2006).
[5] C. F. Pan, H. Wu, C. Wang, B. Wang, L. Zhang, Z. D. Cheng, P. Hu, W. Pan, Z. Y. Zhou, X. Yang, and J. Zhu, J. Adv. Mater. **20**(9), 1644 (2008).
[6] D. Choi, M. Y. Choi, W. M. Choi, H. J. Shin, H. K. Park, J. S. Seo, J. Park, S. M. Yoon, S. J. Chae, Y. H. Lee, S. W. Kim, J. Y. Choi, S. Y. Lee, and J. M. Kim, Adv. Mater. **22**(19), 1 (2010).
[7] A. J. Lovinger, Macromolecules **14**, 322 (1981).
[8] J. B. Lando, H. G. Olf, and A. Peterlin, J. Polym. Sci., Part A **4**, 941 (1966).
[9] A. J. Lovinger, in *Developments in crystalline polymers*, edited by D. C. Basset (Applied Science Publishers Ltd, N. J. Englewood, 1982).
[10] S. Chen, K. Yao, F. E. H. Tay, and C. L. Liow, J. Appl. Phys. **102**, 104108 (2007).
[11] M. G. Buonomenna, P. Macchi, M. Davoli, and E. Drioli, Euro. Polym. J. **43**, 1557 (2007).
[12] X. He and K. Yao, Appl. Phys. Lett. **89**, 112909 (2006).
[13] P. Sajkiewicz, A. Wasiak, and Z. Goclowski, Euro. Polym. J. **35**, 423 (1999).
[14] Z. M. Dang, Y. H. Lin, and C. W. Nan, Adv. Mater. **15**, 1625–1629 (2003).
[15] H. Chen, X. Dong, T. Zeng, Z. Zhou, and H. Yang, Ceram. Inter. **33**, 1369–1374 (2007).
[16] F. M. Dougall, J. Ennis, X. H. Yang, R. A. Copper, J. E. Gilbert, J. F. Bates, T. R. Jow, J. Ho, C. J. Scozzie, and S. P. S. Yen, *IEEE Pulsed Power Conference* (Wshington DC, 2009).
[17] Z. M. Dang, J. K. Yuan, S. H. Yao, and R. J. Liao, Adv. Mater. **25**, 6334 (2013).
[18] V. Tomer, E. Manias, and C. A. Randall, J. Appl. Phys. **110**, 044107 (2011).
[19] Penghao Hu, Yu Song, Haiyang Liu, Yang Shen, Yuanhua Lin, and Ce-Wen Nan, J. Mater. Chem. A **1**, 1688 (2013).
[20] Z. M. Dang, D. Xie, and C. Y. Shi, Appl. Phys. Lett. **91**, 222902 (2007).
[21] Y. Bai, Z. Y. Cheng, V. Bharti, H. S. Xu and Q. M. Zhang, Appl. Phys. Lett. **76**, 3804 (2000).
[22] T. Yamada, T. Ueda, and T. Kitayama, J. Appl. Phys. **53**(6), 4328 (1982).
[23] B. A. Newman, C. H. Yoon, and K. D. Pae, J. Appl. Phys. **50**, 6095 (1979).
[24] S. Chen, K. Yao, F. E. H. Tay, and C. L. Liow, J. Appl. Phys. **102**, 104108 (2007).
[25] G. T. Davis, J. E. Mekinny, M. G. Broadhurst, and S. C. Roth, J. Appl. Phys. **49**(10), 4992 (1978).
[26] K. Tashio and K. Takano, Polymer **24**, 199 (1983).
[27] X. Zheng, Y. Zhou, and Z. Uan, Mat. Res. **4**, 1648 (2003).
[28] Ashok Kumar, R. S. Katiyar, and J. F. Scott, J. Appl. Phys. **108**, 064105 (2010).
[29] R. S. Katiyar, J. F. Ryan, and J. F. Scott, Phys. Rev. B **4**, 2635 (1971).
[30] T. Boccaccio, Bottino, G. Capannelli, and P. Piaggio, J. Membrane Sci. **210**, 315 (2002).
[31] M. Kobayashi, K. Tashiro, and H. Tadokoro, Macromolecules **8**, 158 (1975).
[32] U. Hoffmann, F. Pfeifer, S. Okretic, N. Volkl, M. Zahedi, and H. W. Siesler, Appl Spectr **47**(9), 1531 (1993).
[33] S. Satapathy, S. Pawar, P. K. Gupta, and K. B. R. Varma, Bull. Mater. Sci. **34**, 727 (2011).
[34] B. Mattsson, H. Ericsson, L. M. Torell, and F. Sundholm, J. Polym. Sci A: Polym Chem **37**, 3317 (1999).
[35] V. P. Pavlović, V. B. Pavlović, B. Vlahović, D. K. Božanić, J. D. Pajović, R. Dojčilović, and V. Djoković, Physica Scripta **T157**, 014006 (2013).
[36] Y. Bormashenko, R. Pogreb, O. Stanevsky, and E. Bormashenko, Polym. Testing **23**, 791 (2004).
[37] C. J. L. Constantino, A. E. Job, R. D. Simoes, J. A. Giacometti, V. Zucolotto, Jr., O. N. Oliveira, G. Gozzi, and D. L. Chinaglia, Appl. Spectrosc. **59**, 275 (2005).
[38] A. G. Souza Filho, K. C. V. Lima, A. P. Ayala, I. Guedes, P. T. C. Freire, J. Mendes Filho, E. B. Araújo, and J. A. Eiras, Phys. Rev. B **61**, 14283 (2000).
[39] S. Firmino Mendes, C. M. Costa, V. Sencadas, J. Serrado Nunes, P. Cost, R. Gregorio, Jr., and S. Lanceros-Mendez, Appl. Phys. A **96**, 899 (2009).
[40] M. B. Suresh, T. H. Yeh, C. C. Yu, and C. C. Chou, Ferroelectrics **381**, 80 (2009).
[41] L. E. Nielsen, J. Appl. Polym. Sci. **10**, 97 (1966).
[42] T. Furukawa, J. Aiba, and E. Fukada, J. Appl. Phys. **50**(5), 3615 (1979).
[43] J. Lovinger, T. Furukawa, G. T. Davis, and M. G. Broadhurst, Polymer **24**, 1225 (1983).
[44] R. Gregorio, Jr., M. Cestart, and F. E. Bernardino, J. Mater. Sci., **31**, 2925 (1996).
[45] T. Yamada, T. Ueda, and T. Kitayama, J. Appl. Phys. **53**(6), 4328 (1982).
[46] B. Hilczer, J. Kutek, and E. Markiewicz, Processing of Electroceramics (2003).
[47] O. R. Hughes, J. Polym. Sci. B Polym. Phys. **45**, 3207 (2007).
[48] D. Rollik, S. Bauer, and R. Gerhard-Multhaupt, J. Appl. Phys. **85**, 3282 (1999).
[49] V. Tomer and C. A. Randall, J. Appl. Phys. **104**, 074106 (2008).
[50] V. Tomer, C. Randall, G. Polizos, J. Kostelnick, and E. Manias, J. Appl. Phys. **103**, 034115 (2008).
[51] T. J. Lewis, IEEE Transactions on Dielectrics and Electrical Insulation **11**, 739 (2004).